

GOOD AND BAD BOUNDARIES IN ULTRASOUND COMPOUNDING: PRESERVING ANATOMIC BOUNDARIES WHILE SUPPRESSING ARTIFACTS

Alex Ling Yu Hung^{*} John Galeotti^{†*}

^{*} Department of Biomedical Engineering, Carnegie Mellon University, Pittsburgh PA 15213, USA

[†] Robotics Institute, Carnegie Mellon University, Pittsburgh PA 15213, USA

ABSTRACT

Ultrasound 3D compounding is important for volumetric reconstruction, but as of yet there is no consensus on best practices for compounding. Ultrasound images depend on probe direction and the path sound waves pass through, so when multiple intersecting B-scans of the same spot from different perspectives yield different pixel values, there is not a single, ideal representation for compounding (i.e. combining) the overlapping pixel values. Current popular methods inevitably suppress or altogether leave out bright or dark regions that are useful, and potentially introduce new artifacts. In this work, we establish a new algorithm to compound the overlapping pixels from different view points in ultrasound. We uniquely leverage Laplacian and Gaussian Pyramids to preserve the maximum boundary contrast without overemphasizing noise and speckle. We evaluate our algorithm by comparing ours with previous algorithms, and we show that our approach not only preserves both light and dark details, but also somewhat suppresses artifacts, rather than amplifying them.

Index Terms— ultrasound image compounding, ultrasound anatomic boundaries, ultrasound 3D reconstruction, Laplacian pyramid

1. INTRODUCTION

In ultrasound imaging, it can be hard to see the structures that are deep or underneath some highly reflective surfaces [1]. Sound waves tend to be bounced back or absorbed by certain tissues or structures, resulting in dark regions or artifacts [2]. Some structures or some part of the structure could be difficult to image in a certain direction, preventing clinical doctors from seeing the whole underlying structure. When there are multiple view points available in ultrasound imaging, we can reconstruct 3D volumes that represent the structures that are being imaged. However, creating the 3D volume from 2D sweep is a challenging job. When frames overlap with one another, a way to find the best pixel values to best represent the underlying structures is needed in those overlapped regions.

However, no existing method can do the job perfectly. An averaging approach [3] was first applied to co-planar 3D compounding. Then they reconstructed 3D volumes of freehand

ultrasound images with non-coplanar images by interpolation [4]. The work in [5] showed that the baseline approach in 3D freehand compounding is to calculate the missing pixels with interpolation and the values of overlapping pixels by taking the average. It's found that averaging the different views worked well if the transducer were set up in a certain way [6]. A way to calculate physics-inspired confidence values for each ultrasound pixel is purposed in [7], which [8] used as weights in a uncertainty-based fusion algorithm to compound ultrasound images from different view points. Afterwards, [9] proposed a new way to measure the per-pixel confidence that can improve the compounding results. The works by [10, 11] modeled the 3D reconstruction of ultrasound images based on more complete tensor representations. Nevertheless, these recent methods still average pixel intensities or else take the maximum, while dealing with overlapping pixels.

Our goal is to clearly differentiate all structures, whether dark or bright. Unlike prior work, we are less concerned with recovering the most "accurate" individual pixel values. We focus on preserving patches with the largest contrast, suppressing less-certain high frequency information to prevent piecemeal-stitching artifacts and reduce existing artifacts. Our most important contributions are: (1) Keep the pixels and structures with the higher confidence when compounding. (2) Preserve the pixels or patches that have the largest local contrast among the overlapping values from different viewpoints. (3) Identify anatomic boundaries of structures and tissues and treat them differently while compounding. (4) Use Laplacian pyramid blending [12] to remove discrepancy in pixel values from ultrasound images captured in different view points. (5) Make use of the advantages of different compounding methods in different frequency scales.

2. METHODS

2.1. Identifying Good Boundaries

Any sort of averaging between different views in which an object appears either too bright or dark in one view, will lower the compounded object's contrast with respect to surrounding pixels. Even though artifacts could be suppressed, the useful structures would also be less differentiated, which isn't

the optimal approach. Therefore, identifying good anatomic boundaries, and treating them differently than other pixels while compounding, is essential to preserving the dynamic range and contrast of the image.

Ultrasound transmits sound waves in the axial (e.g. vertical) direction, so sound waves are more likely to be bounced back by horizontal surfaces. Horizontal edges in particular should be examined to determine whether or not they are artifacts, and in particular reverberation artifacts [13]. The trait of reverberation artifacts is that the position where the true object lies is the brightest at the top, then a few artificial lines appear beneath it. One observation is that the distance between the detected edges of reverberation artifacts are usually shorter than other structures. Also, structures in ultrasound images are usually not a single line of pixels, they usually have thickness. Thus if we don't have enough data or labels to train an artifact segmentation network like [14], we can refine the detected edges as follows:

Algorithm 1: Horizontal-edge refinement

Data: input image I
Result: output boundary mask B
 $edges = clustering(denoising(\frac{dI}{dy}));$
 $mask = zeros(I.shape); B = zeros(I.shape);$
for $edge$ **in** $edges$ **do**
 if $\forall e$ **in** $edges$ **that are far enough from edges**
 underneath then
 $mask[edge] = 1;$
for $[i, j]$ **where** $mask[i, j] == 1$ **do**
 if $B[i, j] == 0$ **then**
 stack s ; # initialize stack
 if $I[i, j] > threshold1$ **then**
 $s.push([i, j]); B[i, j] = 1;$
 while s **is not empty do**
 $[x, y] = s.pop;$
 for $[ii, jj]$ **in the neighborhood of** $[x, y]$ **do**
 if $I[ii, jj] > threshold1$ **and**
 $|I[x, y] - I[ii, jj]| < threshold2$
 and $B[ii, jj] == 0$ **then**
 $s.push([ii, jj]); B[ii, jj] = 1;$

2.2. Compounding Algorithm

Attenuation reduces ultrasound image contrast in deeper regions. Simply taking the maximum, median or mean while compounding [15] further undermines the contrast information, where structure information is stored. Taking the maximum also would create artifacts by emphasizing non-existent structures resulting from noise in uncertain regions. The uncertainty compounding approach from [8] produces substantially darker images than the originals, lowering the dynamic

ranges. Even though taking the maximum retains the bright regions, some dark regions are also meaningful, so it would make more sense if the patches with the largest local contrast instead of the maximum pixel values can be preserved. However, directly taking pixels with the largest contrast would lead to neighboring pixels inconsistently alternating between different source images. Besides, the neighbors of a pixel might all be noise, resulting in instability of the algorithm.

We developed a novel Laplacian-pyramid [12] approach to compound the images at different frequency bands and different scales. Therefore, we can apply contrast maximization method above certain frequency bands while reconstructing from the pyramid. However, at extremely large scale, one pixel could represent hundreds of pixels, so the maximum weighted contrast patch there would consist of a lot of structures, which would be useless. On the other hand, when the scale is small, the neighborhood contrast around a single pixel might all be noise, causing the above maximum weighted contrast to introduce new artifacts into the image. At extremely low and high scales, we thus observe contrast to be less important than intensity confidence measures. Another flaw of directly maximizing the contrast is that the large contrast region might contain artifacts and shadows, so we only maximize the contrast when the overlapping pixels have similar structural confidence values [9], otherwise we take the pixel with the larger structural confidence value, as low structural confidence value indicates artifacts or shadows.

Our novel ultrasound compounding method takes ultrasound images from multiple view points and calculates their intensity and structural confidence maps[9], then calculates Laplacian and Gaussian[16] pyramids of the original images and the Gaussian pyramid of confidence maps. Denote $L_{m,n}$ $GI_{m,n}$ as the n^{th} layer of the Laplacian pyramid and Gaussian pyramid of the m^{th} co-planar ultrasound image respectively. $GC_{m,n}$ $G\Gamma_{m,n}$ as the n^{th} layer of the Gaussian pyramid of the intensity and structural confidence map of m^{th} co-planar ultrasound image respectively, and, L_k as the k^{th} layer of the Laplacian pyramid of the synthetic image. M is the set of viewpoints, with $|M|$ views. Also denote $N(i, j)$ the 8-connected neighborhood of pixel (i, j) . Here we combine the weighted maximum contrast and weighted average together. For the k^{th} layer of the pyramid, if the difference across viewpoints between the maximum and minimum structural confidence values $G\Gamma_{m,k}(i, j)$, where $m \in M$, is less than a certain threshold, we take the pixel (i, j) with the largest contrast at this scale, since only when there is no artifact at the pixel does taking the largest contrast make sense

$$\tilde{m}(i, j) = \arg \max_{m \in M} \sum_{(a,b) \in N(i,j)} |GI_{m,k}(a, b) - GI_{m,k}(i, j)| \quad (1)$$

If not, we take the pixel (i, j) with the largest structural confidence at this scale

$$\tilde{m}(i, j) = \arg \max_{m \in M} G\Gamma_{m,k}(i, j) \quad (2)$$

Denote the intensity-confidence weighted average at the k^{th} layer of the Laplacian pyramid as La_k ,

$$La_k(i, j) = \frac{\sum_{m=1}^{|M|} GC_{m,k}(i, j) L_{m,k}(i, j)}{\sum_{m=1}^{|M|} GC_{m,k}(i, j)} \quad (3)$$

Then the k^{th} layer of the Laplacian pyramid of the synthetic image can be calculated as,

$$L_k(i, j) = \phi(k) L_{\tilde{m}(i,j),k}(i, j) + (1 - \phi(k)) La_k(i, j) \quad (4)$$

where

$$\phi(k) = \frac{1}{0.4\sqrt{2\pi}} e^{-\frac{1}{2} \left(\frac{(2k-K-1)^2}{0.16(K-1)^2} \right)} \quad (5)$$

is a weight function, and K is the number of total layers. This weight function is designed to assign lower weights to contrast maximization and higher weights to intensity-confidence-weighted average in extremely low and high scale.

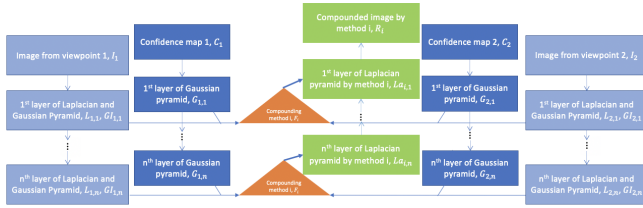


Fig. 1. compounding with Laplacian and Gaussian pyramid

The compounding algorithm could be further generalized:

$$L_k(i, j) = \sum_{n=1}^N \phi_n(k) F_n(\{L_{m,k}\}_{m \leq |M|}, \{G_{m,k}\}_{m \leq |M|}) \quad (6)$$

where

$$\sum_{n=1}^N \phi_n(k) = 1, 0 < k \leq K, 0 < n \leq N, 0 \leq \phi_n(k) \leq 1 \quad (7)$$

K is the total number of layers, N is the total number of compounding methods, p is the total number of view points, $G_{m,k}$ denote any kind of confidence map at layer k from view point m , and F_n denote a compounding method.

We can use any weighting scheme to combine any number of compounding schemes in the Laplacian pyramid, based on what the needs are and what the data look like.

Even though this approach works well, the actual boundaries of structures tend to get darker. In addition to what we just proposed above, the algorithm we purposed back in section 2.1 can also be incorporated. While reconstructing the image from the new Laplacian pyramid after getting the image from the third layer, the good boundaries are detected and values from the original images are taken. For overlapping pixels here, we take the average. We apply the same notation as above, and $GB_{m,k}$ is layer k from viewpoint m of the

Gaussian pyramid of the boundaries mask B (Gaussian pyramid of algorithm 1's output).

$$L_3(i, j) = \max\left(\frac{\sum_{m=1}^{|M|} GB_{m,3}(i, j) GI_{m,3}(i, j)}{\sum_{m=1}^{|M|} GB_{m,3}(i, j)}, L_3(i, j)\right) \quad (8)$$

This step is done on the third layer of the pyramid since there are still two layers before the final output, so piecemeal-stitching artifacts can still be suppressed. The step isn't done in deeper layers, so that we can still preserve contrast.

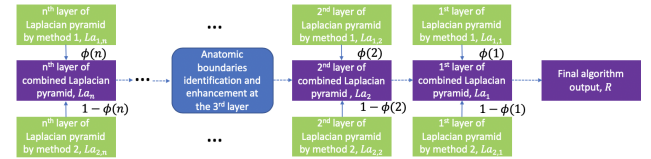


Fig. 2. pipeline for combining two individual compounding methods and boundaries enhancement

3. EXPERIMENTS

The ultrasound imaging is performed by UF-760AG Fukuda Denshi diagnostic ultrasound imaging equipment and Diasus High Frequency Ultrasound, on an lamb heart and an anthropomorphic phantom produced by Advanced Medical Technologies with a needle inserted in it.

3.1. Qualitative Evaluation

We visually compare the results of our method against average [3], maximum [15], and uncertainty-based fusion [8]. As is shown in Fig. 3, our algorithm has the best result in suppressing artifacts, and at the same time, the brightness of the boundaries (green arrows) from our algorithm is similar to that of taking maximum [15]. Our method also preserves a lot more contrast since other parts of the patch are darker in comparison to our bright boundaries, whereas the boundaries from the other two compounding algorithms are darker and therefore less contrasting with the dark interior. Our algorithm also completely suppresses the reverberation artifacts in the regions that the red and yellow point to, while the results from other algorithms all preserve undesirable aspects of artifacts.

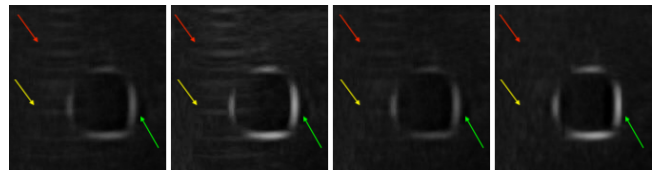


Fig. 3. Compounded patches left to right: average [3], maximum [15], uncertainty-based fusion [8], and our algorithm

More qualitative comparison is shown in Fig. 4. The first five rows are results on the phantom while the last row are the results on a lamb heart. In the first row, our algorithm almost completely removes the reverberation artifacts in the synthesized image and at the same time preserves the contrast in the images. In other phantom examples, our algorithm also is the best in removing the reverberation artifacts and shadows the vessel walls cast, while preserving the brightness of the vessel walls, needles and other structures in the images. Our algorithm preserves the "good boundaries" that represent the anatomic boundaries while suppressing boundaries that are not real. In the lamb heart example, only maximum [15] preserves the contrast at the red arrows, but fails to preserve the contrast at the blue arrows, while our method keeps the contrast at both red and blue arrows.

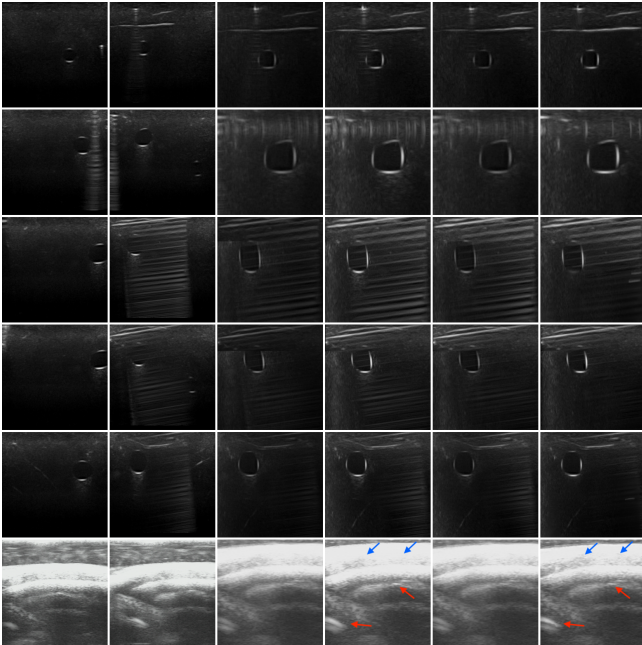


Fig. 4. The first five rows are results on phantom with a needle inserted in it, and the last row are on a butcher-shop lamb heart in a water bath. The left two columns are the two input images (phantom images were acquired orthogonally within plane). The right four columns from left to right are zoomed-in results from average [3], maximum [15], uncertainty-based fusion [8], and our algorithm. Our method best preserves bright and dark anatomy while suppressing artifacts.

3.2. Quantitative Evaluation

We continue to compare our results with average (avg) [3], maximum (max) [15], and uncertainty-based fusion (UBF) [8]. We separately evaluate image patches containing artifacts, which should have low contrast, and patches containing boundaries, which should have high contrast. For the patches

with artifacts, we evaluated the algorithms based on the ratio between the variance of the patch and the variance of the whole image, and the ratio between the mean of the patch and the mean of the whole image. The patches with the artifacts should have lower variance and a similar mean compared with the whole image, since artifacts are supposed to be suppressed. As for patches with real boundary signals, we only care about the contrast, so our metric is only the ratio between the variance of patch and the whole image. We want the variance in the patches with boundary signals to be much larger than the variance of the whole image. The results are listed in Table 1 of average mean ratio (AMR) and average variance ratio (AVR) metrics. Our method outperforms other algorithms in suppressing artifacts. As for real boundary signals, our method appears superior to all the other methods.

Table 1. Evaluation by Mean and Variance

		avg	max	UBF	ours
artifacts	AMR	1.757	1.433	1.277	1.206
	AVR	0.204	0.234	0.134	0.048
boundaries	AVR	3.007	3.612	1.696	3.876

Additionally, we also compare our results with the previous ones by performing vessel segmentation on the compounded images. We manually selected the patches containing vessels and annotated the vessel boundaries as ground truth. Otsu thresholding [17] was applied to each compounded patch to automatically separate the vessel boundaries, and we then fit an ellipse to segment the vessel. Table 2 shows dice coefficients [18] comparing each method against ground truth. This simple adaptive segmentation showed that our results were better than the prior algorithms at preserving the vessel walls while suppressing noise and artifacts.

Table 2. Evaluation by Segmentation

	avg	max	UBF	ours
Dice Coefficient	0.878	0.883	0.874	0.901

4. CONCLUSION

In this work, we presented a new ultrasound compounding method based on confidence, contrast, and both Gaussian and Laplacian pyramids, taking into account the direction of ultrasound propagation. Our approach appears better at preserving contrast at anatomic boundaries while suppressing artifacts than any of the other compounding approaches we tested. With what we have achieved in this work, we hope our method could become a benchmark for ultrasound compounding and inspire others to build upon our work. Potential future work that could be built upon ours includes 3D volume reconstruction, needle tracking and segmentation, artifacts removal and identification, etc.

5. COMPLIANCE WITH ETHICAL STANDARDS

This study used only phantoms and grocery-store butcher tissue, for which no ethical approval was required.

6. ACKNOWLEDGMENTS

This work was sponsored in part by US Army Medical contracts W81XWH-19-C0083, W81XWH-19-C0101, and W81XWH-19-C-0020, and by a PITA grant from the state of Pennsylvania DCED C000072473. We thank our collaborators at the University of Pittsburgh, Triton Microsystems, Inc., Sonivate Medical, URSUS Medical LLC, and Accipiter Systems, Inc. We are pursuing intellectual-property protection. Galeotti serves on the advisory board for Activ Surgical, Inc., and he is a Founder and Director for Elio AI, Inc.”

7. REFERENCES

- [1] Jørgen Arendt Jensen, “Linear description of ultrasound imaging systems: Notes for the international summer school on advanced ultrasound imaging at the technical university of denmark,” 1999.
- [2] Frederick W Kremkau and KJ Taylor, “Artifacts in ultrasound imaging,” *Journal of ultrasound in medicine*, vol. 5, no. 4, pp. 227–237, 1986.
- [3] Jason W Trobaugh, Darin J Trobaugh, and William D Richard, “Three-dimensional imaging with stereotactic ultrasonography,” *Computerized Medical Imaging and Graphics*, vol. 18, no. 5, pp. 315–323, 1994.
- [4] Robert Rohling, Andrew Gee, and Laurence Berman, “A comparison of freehand three-dimensional ultrasound reconstruction techniques,” *Medical image analysis*, vol. 3, no. 4, pp. 339–359, 1999.
- [5] Mohammad Hamed Mozaffari and Won-Sook Lee, “Freehand 3-d ultrasound imaging: a systematic review,” *Ultrasound in medicine & biology*, vol. 43, no. 10, pp. 2099–2124, 2017.
- [6] Vera Behar and Milen Nikolov, “Statistical analysis of image quality in multi-angle compound imaging,” in *IEEE John Vincent Atanasoff 2006 International Symposium on Modern Computing (JVA’06)*. IEEE, 2006, pp. 197–201.
- [7] Athanasios Karamalis, Wolfgang Wein, Tassilo Klein, and Nassir Navab, “Ultrasound confidence maps using random walks,” *Medical image analysis*, vol. 16, no. 6, pp. 1101–1112, 2012.
- [8] Christian Schulte zu Berge, Ankur Kapoor, and Nassir Navab, “Orientation-driven ultrasound compounding using uncertainty information,” in *International conference on information processing in computer-assisted interventions*. Springer, 2014, pp. 236–245.
- [9] Alex Ling Yu Hung, Wanwen Chen, and John Galeotti, “Ultrasound confidence maps of intensity and structure based on directed acyclic graphs and artifact models,” in *2021 IEEE 18th International Symposium on Biomedical Imaging (ISBI 2021) (under review, submission 444, will post on arXiv once IP is filed)*. IEEE.
- [10] Christoph Hennemersperger, Maximilian Baust, Diana Mateus, and Nassir Navab, “Computational sonography,” in *International conference on medical image computing and computer-assisted intervention*. Springer, 2015, pp. 459–466.
- [11] Rüdiger Göbl, Diana Mateus, Christoph Hennemersperger, Maximilian Baust, and Nassir Navab, “Redefining ultrasound compounding: Computational sonography,” *arXiv preprint arXiv:1811.01534*, 2018.
- [12] Peter J Burt and Edward H Adelson, “A multiresolution spline with application to image mosaics,” *ACM Transactions on Graphics (TOG)*, vol. 2, no. 4, pp. 217–236, 1983.
- [13] Mary M Quien and Muhamed Saric, “Ultrasound imaging artifacts: How to recognize them and how to avoid them,” *Echocardiography*, vol. 35, no. 9, pp. 1388–1401, 2018.
- [14] Alex Ling Yu Hung, Edward Chen, and John Galeotti, “Weakly- and semi-supervised probabilistic segmentation and quantification of ultrasound needle-reverberation artifacts to allow better ai understanding of tissue beneath needles,” *Robotics and Automation Letter (under review, will post on arXiv once IP is filed)*.
- [15] Andras Lasso, Tamas Heffter, Adam Rankin, Csaba Pinter, Tamas Ungi, and Gabor Fichtinger, “Plus: open-source toolkit for ultrasound-guided intervention systems,” *IEEE transactions on biomedical engineering*, vol. 61, no. 10, pp. 2527–2537, 2014.
- [16] Alexander Toet, “Image fusion by a ration of low-pass pyramid,” *Pattern Recognition Letters*, vol. 9, no. 4, pp. 245–253, 1989.
- [17] Nobuyuki Otsu, “A threshold selection method from gray-level histograms,” *IEEE transactions on systems, man, and cybernetics*, vol. 9, no. 1, pp. 62–66, 1979.
- [18] Kelly H Zou, Simon K Warfield, Aditya Bharatha, Clare MC Tempany, Michael R Kaus, Steven J Haker, William M Wells III, Ferenc A Jolesz, and Ron Kikinis, “Statistical validation of image segmentation quality based on a spatial overlap index1: scientific reports,” *Academic radiology*, vol. 11, no. 2, pp. 178–189, 2004.